Performance of a Horizontally Scanning Doppler Sonar near Shore

JEROME A. SMITH

Scripps Institution of Oceanography, La Jolla, California

(Manuscript received 12 August 1992, in final form 4 January 1993)

ABSTRACT

In August 1990, tests were performed to investigate the usefulness of a horizontally scanning Doppler acoustic technique in shallow water. Comparisons of radial velocity estimates from a vertical fan beam versus a horizontally aimed pencil beam indicate no degradation attributable to multiple reflections from the surface and bottom. Further tests, in which ping-to-ping phase-coherent means are examined, indicate negligible stationary backscatter from the bottom. Tests in which the acoustic beams were directed shoreward indicate that an extremely dense bubble cloud formed by plunging breakers produces an impenetrable "wall" at the breakpoint, at acoustic frequencies near 195 kHz. Useful velocity estimates (one component) are obtainable everywhere seaward of the breakpoint of the incoming surf. The spatially extensive velocity estimates offered by this technique provide enormous potential for the study of horizontal currents and wave–current interactions in shallow water.

1. Introduction

Phenomena such as rip currents, alongshore flows, tidal "jets" from inlets, and interactions between each of these and the incident wave field are ubiquitous in the nearshore regime (e.g., Inman and Brush 1973) yet are still poorly understood. To investigate these phenomena, mapping of waves and currents over a substantial time and area is needed. However, measurement of surface waves and currents in the nearshore regime remains a significant challenge. While pressure sensors serve to describe the surface wave field (e.g., Herbers and Guza 1991, 1992), deployments of current meters in two- or three-dimensional arrays are rather more difficult and are quite susceptible to environmental disturbances (e.g., destruction by breaking waves or by moving sandbars).

A recent comparison of a compact acoustic Doppler current meter with pressure-array measurements yielded excellent quantitative agreement (Herbers et al. 1991). The Doppler system described there consists of four upward-looking beams. The rangewise (slanted) component of velocity is tracked at four fixed points below the surface. Herbers et al. show that this system yields directional wave estimates comparable to those from a tilt-and-roll buoy. There is also potential to extract vertical profiles of the currents above the instrument, without requiring structures in the water column that could interfere with the flow. For the purposes outlined above, however, there remains the difficulty of deploying a large horizontal array of such current measuring systems.

Here, a horizontally scanning Doppler acoustic technique is described and investigated for use near shore. This approach has proven useful in the study of waves and Langmuir circulation in the open ocean (e.g., Smith 1992). In this approach, vertically fan-shaped beams intersect the surface along lines up to a kilometer long (depending on the acoustic frequency used). As each transmitted "ping" scans along a line, the backscatter is processed to yield contiguous estimates of the rangewise component of velocity. An advantage of this approach is that radial velocity measurements can be obtained in a fairly dense pattern over a sizable horizontal extent, from a single location. For example, measurements can be obtained every 3 or 4 m along 350-m lines radiating from a single instrument package, every 0.5 s or so, using 200-kHz sound. It would be useful to obtain such temporally and spatially extensive measurements in the nearshore environment; however, it was not previously known how well such an acoustic Doppler system would work in shallow water. For example, it was feared that multiple reverberations from both the surface and the bottom would degrade the signal and introduce confusion about the location from which the velocity estimates arise. A narrow "pencil" beam minimizes the occurrence of multiple reverberations yet introduces more sensitivity to the tilt of the package and, hence, to environmental disturbances. Conversely, a vertical fan beam is insensitive to the angle of the instrument but would be more susceptible to multiple reverberations should these prove to be a problem.

The horizontally scanning Doppler system provides information about the radial velocity over a vertically

Corresponding author address: Dr. Jerome A. Smith, Marine Physical Laboratory, Scripps Institution of Oceanography, La Jolla, CA 92093-0213.

weighted integral of the water column. It does not provide information about the vertical structure of the velocity field. It is a good complement to existing and developing techniques for measuring the vertical structure at a few locations. Interpretation of the vertical measurements would benefit from measurements of the 2D horizontal "context," and vice versa. The acoustic intensity of the backscatter is also of some interest, as many features can be deduced from examination of this data. Side-scan sonars have previously been put to use in moderate depth water to examine the characteristics of breaking waves and bubble clouds (e.g., Thorpe and Hall 1983). More recently, Thorpe and Hall (1993) have deployed a side-scan sonar near shore and examine intensity returns under circumstances similar to those described here.

A series of tests in the summer of 1990 was designed to investigate the performance of a vertical fan beam in shallow water. The results indicate that neither multiple reverberations nor direct backscatter from the bottom is a problem, under the conditions of the tests (most notably, with winds consistently over 5 m s^{-1} or so). The velocity estimates appear to be dominated by backscatter from bubbles near the surface, as is the case in deep water. Usable velocity estimates can be obtained anywhere seaward of the breakpoint of the incoming surface waves.

The tests employed a single "look direction," which is adequate to address the initial questions concerning the feasibility of the approach. It is worth noting, however, that the technology now exists to synthesize many contiguous beams, covering a "wedge" of at least 45°, from a single location. Such a system was recently deployed as part of Arctic Leads Experiment (LEADEX), which took place in the Arctic in the spring of 1992. This system employs 16 receivers, with 26 spatial lags, and monitors velocities over a wedge 44° wide with over 50 (nonindependent) digitally synthesized beams.

2. Experimental setup

The tests described here were conducted in August 1990 from a pier located in La Jolla, California, (Fig. 1). The instruments were deployed on the south side of the pier, near the end, in water about 5 m deep (±1 m, depending on the tide). The transducers and electronics used are from a system developed for the Surface Wave Process Program (SWAPP, Weller et al. 1991; Smith 1992). This horizontally scanning Doppler sonar system was designed to monitor surface velocities in deep water, to track both surface wave orbital velocities and the lower-frequency motions (cf. Smith 1989, 1992). This system operates at a center frequency of 195 kHz. The transducers are bars about 1.47 cm × 50.1 cm. The calculated one-way beam pattern is about 26° vertically by 0.8° azimuthally (to −3-dB points). A pencil beam was synthesized by receiving the same backscattered signal on a transducer rotated 90°, so the received beam pattern is 26.4° in the horizontal by 0.77° in the vertical. The net beam pattern

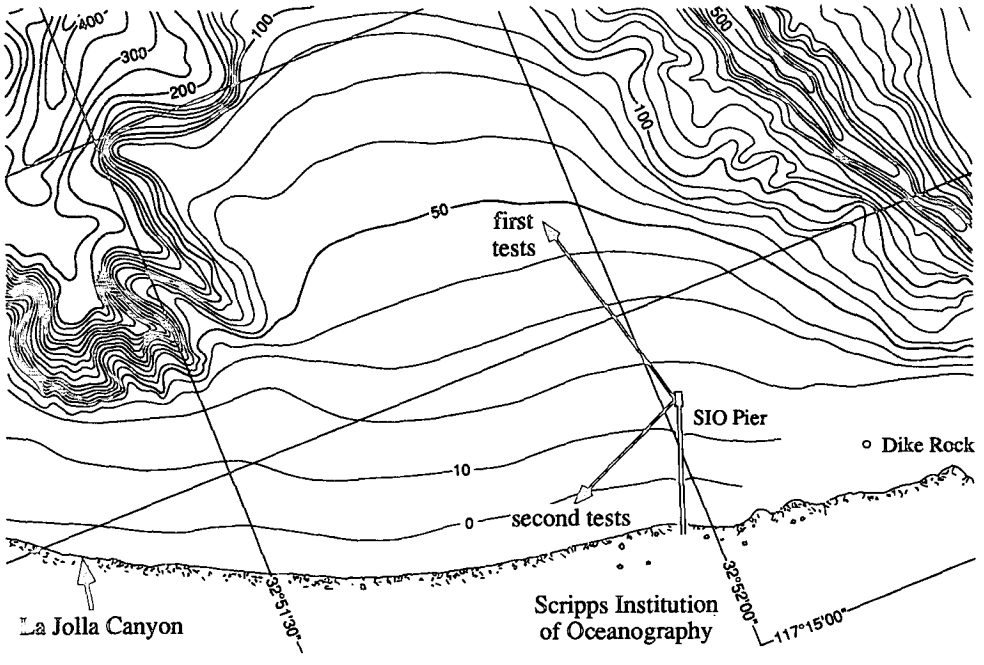

FIG. 1. Plan view of the sonar beams in each of the two orientations used during the tests, roughly to scale. The depth contours are in feet below mean monthly low water. At the location of the instrument, the water depth is about 5 m, ±1 m of tide. The tests took place in August 1990.

is the product of the transmitted and received beam patterns, and is roughly 19.0° × 0.55° for the vertical fan, or 0.77° × 0.77° for the pencil beam (see Fig. 2). This setup has the advantage that the fan and pencil beams are derived from the same transmissions.

Velocity estimates were formed by the standard complex autocovariance technique, as modified for pulse-to-pulse incoherent, repeat-sequence coded sonars (Pinkel and Smith 1992). The "normal" operating bandwidth was 5 kHz (bit lengths of 0.2 ms). Uncoded (1-bit), 4-bit, and 7-bit coded transmissions were tried, with the 4-bit length used most commonly. Exceptions to this "normal operation" are noted in context. The averaging times and pulse durations were held nearly constant, such that $T_{avg} = T_{overlap} \approx 4$ ms (20 bits for the uncoded and 4-bit cases, 21 bits for the 7-bit case). This corresponds to 3-m range resolution. For reference, the theoretically estimated rms error of the velocity estimates with the 4-bit code is about 9 cm s^{-1} per range bin per transmission (ping), while in practice it is seen to be closer to 12 cm s^{-1} (Pinkel and Smith 1992).

In deep water, the acoustic return is normally dominated by backscatter from bubbles. At 195 kHz the resonant bubble size is about 15 μm. For a vertical fan beam, the vertical extent of the measurement volume is normally confined by the form of a near-surface "bubble layer" and bubble clouds. The average intensity of the backscatter from this near-surface layer, when present, is found to be 25–45 dB greater than returns from below the surface or when it is absent. This bubble layer is continuous (but variable) in winds over 3–4 m s^{-1} and dominates the backscatter signal. The bubbles are believed to remain strongly surface trapped, both inside and outside the denser bubble clouds, with a profile roughly equivalent to exponential decay having a depth scale of about 1–1.5 m (Thorpe 1986; Crawford and Farmer 1987). The same depth scale applies to the vertical weighting of the sonar measurements from the vertical fan beam. This beam geometry minimizes sensitivity to tilting of the instrument while maintaining measurement volumes of about $(3\ m)^3$ just below the ocean surface. The measurements follow the vertical excursions of the fluid, to the extent allowed by geometry. The resulting measurements are "semi-Lagrangian," following fluid parcels in the vertical but not in the horizontal directions.

In shallow water, sound can also scatter off the bottom. This can result in 1) a signal component with near-zero Doppler shift, arising from direct reflections off the bottom, and 2) multiple reflections between the surface and bottom, potentially complicating the interpretation of the returns (Fig. 3). In anticipation of problem 1, a processing algorithm was implemented that allows for the examination and removal of a stationary signal. If (say) the direct bottom reflections are sufficiently stationary, a phase-coherent profile can be formed from an average over several transmissions

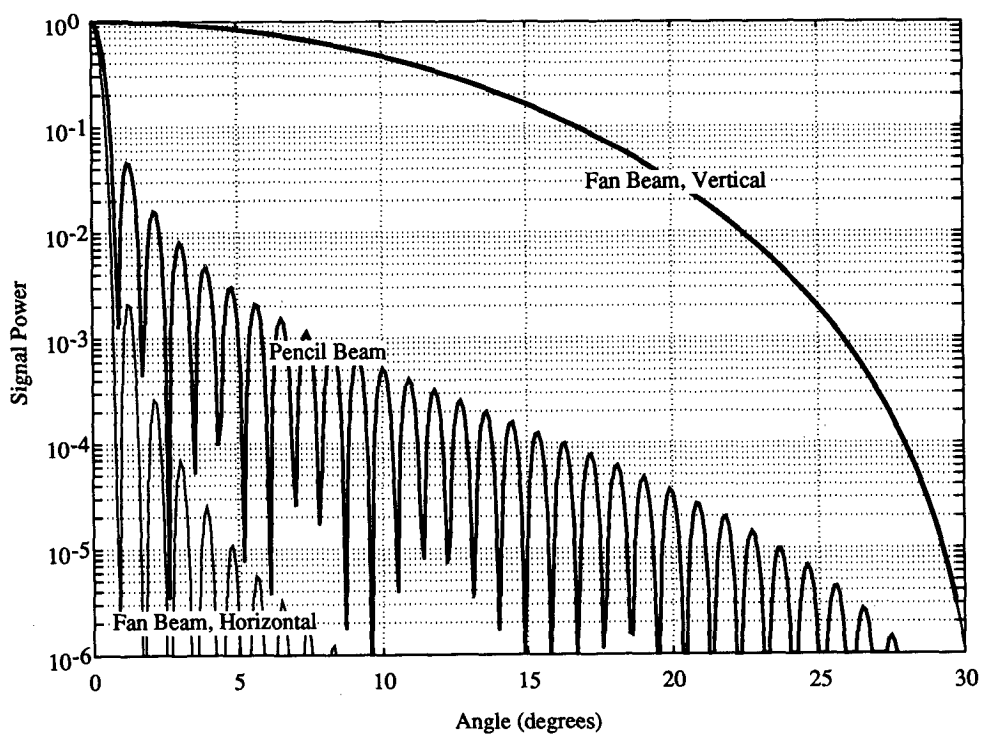

FIG. 2. Ideal beam patterns for the transducers used. Plotted is the net signal power including both transmit and receive patterns.

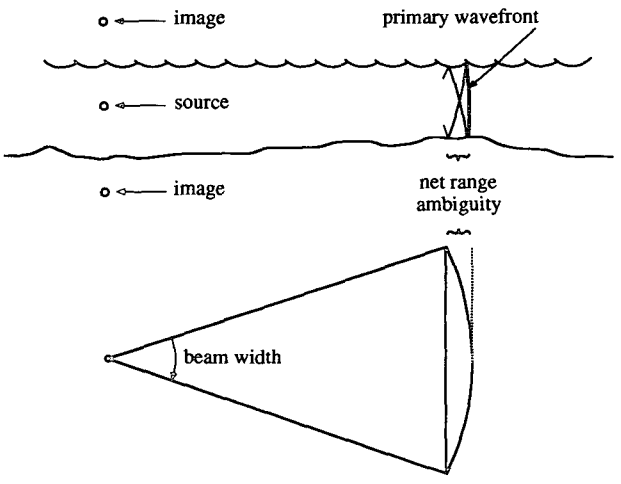

FIG. 3. Schematic illustration of the effects of reflections from the surface and bottom. (Several additional possible paths are not shown, for simplicity.) The net effect of multiple bounces is to broaden the range interval from which the instantaneous signal is received. The broadening is always toward the instrument relative to the "nominal range" calculated from the time of travel.

and removed prior to incoherent processing. The results from this method are compared to those obtained with no "coherent mean" removal scheme. As we shall see, the magnitude of the coherent mean signal is small. The second problem (multiple reflections) is addressed by comparison of vertical fan-beam results with those from a pencil beam. Multiple reverberations should result in estimates from a region effectively "smeared" in range toward the instrument (Fig. 3). This should result in a systematic difference between the estimated signal from the fan beam and from the pencil beam, both with increasing range and as the wavelength of the surface waves generating the signal decreases (i.e., with increasing surface wave frequency). Again, the measured effect appears negligible, indicating weak or no influence from reflections.

In the first few tests, the beams were directed 45° seaward and southward from near the end of the pier, over a relatively flat bottom (Fig. 1). This provides 1) an estimate of the total range achievable with the system in shallow water, and 2) a maximal range interval over which the above comparisons may be made (and hence, ultimately, more degrees of freedom). Another set of tests was run with the beams directed 45° shoreward to see 1) whether a shoaling bottom results in increased interference due to multiple reflections, and 2) how far shoreward the velocity signal remains usable.

3. Coherent backscatter

Reflections from the bottom should be nearly stationary from ping to ping; that is, the backscatter from the bottom should be phase coherent over several seconds (given a phase-coherent signal). Of course, sand can move along the bottom. However, the conditions during the tests described here were mild, and the sonar beams were (initially) aimed seaward, from well outside the wave breakpoint. For at least part of each wave period there should be times when the bottom is stationary.

The first set of tests explores the possibility that some fraction of the backscatter is phase coherent for times longer than the interval between pings. For these tests, the transmission interval was reduced to 0.25 s in order to maximize the possibility of detecting such "ping-to-ping coherence." Also, since the coherent-mode computations to be described are rather more computationally intensive, the sample rate was reduced to 2 hHz (0.5-ms interval). Uncoded transmissions of nine sample durations were made, and the resulting covariances were averaged over eight consecutive samples in range. A total of 66 "blocks" of 16 pings each was used for this analysis, recorded consecutively on the afternoon of 11 August 1990. These tests require a system with phase stability and reproducibility over fairly long times; the present system is a descendent of the one used by Sherman and Pinkel (1991) for coherent processing and so has field-proven capability in this regard.

Phase-coherent averages were formed over data "blocks" of 4 s (16 pings). The "coherent mean" so formed was stored separately for each block. The amplitude of the coherent mean yields a measure of the signal power that is coherent over the whole 4-s block of data or longer. In practice, statistical sampling error is important, since it is found that the coherent mean intensity is small compared to the total intensity. The predicted level of "coherent mean intensity" is just one-sixteenth of the total intensity (−12 dB), with the assumption of no true coherence over that time scale. Figure 4 shows average profiles versus range of total intensity and the coherent mean intensity, for both the vertical fan and pencil beams. The ratio of the coherent mean intensity to the total intensity is shown in Fig. 5. The expected level is about −12 dB (for sample error with no true correlation).

A "coherent-mode" covariance was also formed and averaged over the 16-ping blocks. In this mode, a covariance is formed over a time lag exactly equal to the transmission interval (cf. Lhermitte and Serafin 1984). Thus, the net phase of backscatter from each range cell is compared to that from the same range cell one ping later (0.25 s). This approach requires coherence over the 0.25-s interval between sequential pings rather than over the whole 4-s block. The magnitude of the coherent-mode covariance, compared to the overall intensity ("coherent-mode coherence"), yields a measure of the signal power that is coherent over 0.25 s or more. Again, statistical sample error must be taken into account. For this case, the predicted (null-hypothesis) level is one over the square root of the number of samples, or 0.25 (Fig. 6).

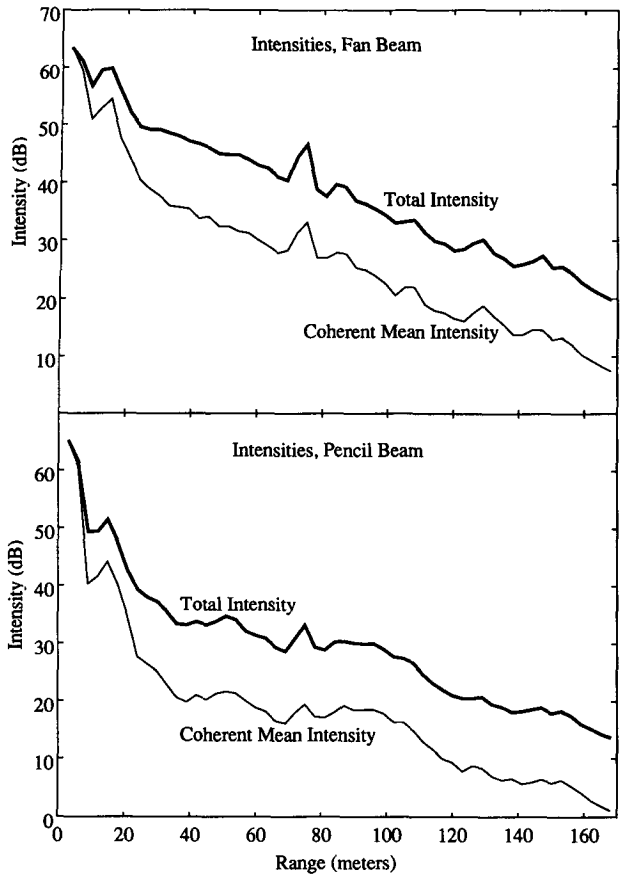

FIG. 4. Acoustic intensity (dB) versus range (m) from the two beam configurations. The pencil beam initially "misses" the surface, so that attenuation is offset against the effect of the beam pattern including more of the (stronger) near-surface backscatter (e.g., over ranges 40–100 m). In contrast, the fan beam fades steadily with range, in accordance with acoustic attenuation. The "bump" in intensity at about 75-m range is probably due to a patch of seaweed floating on the water.

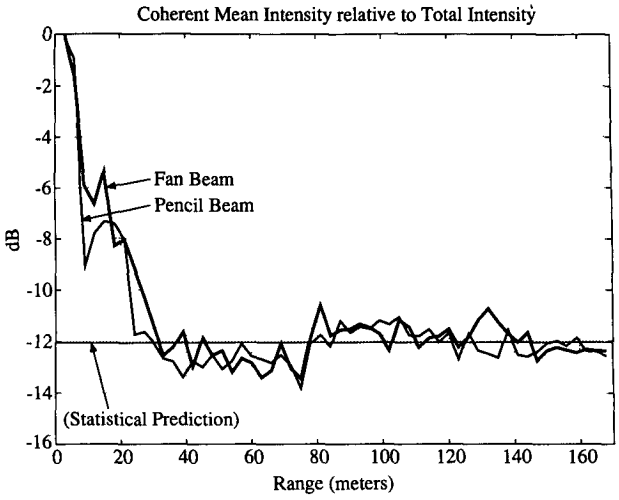

FIG. 5. Intensity associated with a 4-s "coherent mean," relative to the total intensities of Fig. 4 (see text). The strength of the coherent signal computed from 4-s means is no bigger than would be expected due to random "sample error" from an incoherent signal.

Finally, the coherent mean profiles were subtracted from each corresponding 16-ping block of data, and the residual was processed with the "standard" incoherent scheme described above. This scheme requires only coherence over times of order 0.5 ms, as configured here. The "incoherent-mode" covariance magnitude is also compared to the total intensity ("incoherent-mode coherence"). For the particular operating parameters of this test, the expected maximum coherence is 8/9 (which would imply 100% true signal coherence over 0.5 ms); some reduction is expected due to the finite coherence times, even relative to 0.5 ms (Fig. 6). In fact, the observed coherences generally fall near the maximum. There is no discernible difference in the incoherent-mode results from before versus after the removal of the 4-s coherent mean.

Coherence was tested for over time scales of 0.0005, 0.25, and 4 s. Significant coherence is found only at the shortest time scale.

The motivation for "coherent mean removal" is to subtract out bottom scatter, allowing the backscatter from the interior of the water to be processed separately. However, this appears unnecessary. In fact, removal of means based on a few profiles can make the estimates more noisy rather than less, owing to the statistical error in determining the means. The above analysis indicates no detectable signal with coherence times as long as 0.25 s.

Finally, it should be noted that these tests were conducted with about 5 m s^{-1} winds and with gentle whitecapping. It is possible (indeed, it is strongly sug-

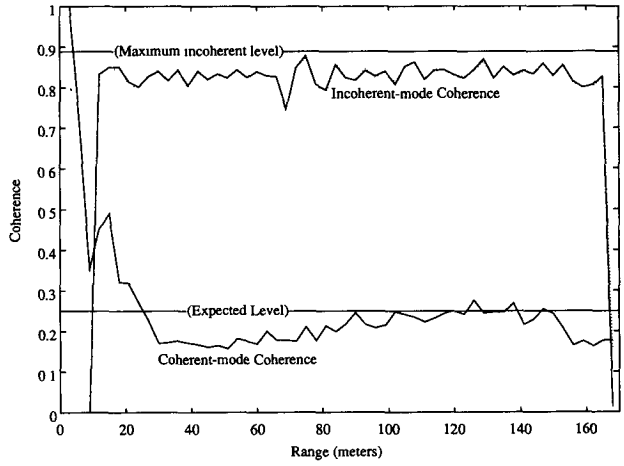

FIG. 6. Coherence levels for both an "incoherent mode" (formed from samples adjacent in range) and a "coherent mode" (formed from samples at the same range but from consecutive transmissions). The coherence at a time lag of one ping (0.25 s) is not significantly different from that expected due to sample error with no true coherence.

gested by some newer data) that at lower wind speeds the bottom reflections could be detected.

4. Fan beam versus pencil beam

Even though direct coherent returns from the bottom appear to be negligible, there could still be effects due to multiple reflections between the surface and bottom (Fig. 3). The absence of coherent backscatter fails to prove absence of bottom backscatter. "Glancing bounces" off the bottom, which are then backscattered from bubbles just below the surface, yield the velocity near the surface. The displacement in range would not be large (though perhaps detectable) since the sonar is only 1 m off the bottom. In this respect, such glancing bounces do not affect the interpretation of the data as representing surface or near-surface velocities. However, another possible way by which bottom backscatter can become "incoherent" is through variations in the sound speed over the range to and from the measurement distance, between pings. In the presence of bubbles, such variations may quite plausibly exist. In either case, it is worthwhile to compare the pencil-beam versus the fan-beam results.

A reasonable way to compare the two beams is to examine cross-spectra formed between the data from the two kinds of beam. However, as can be seen from a time–range display of velocities (Fig. 7), there is considerable noise variance combined with the signal from surface waves. It is therefore worthwhile to find some way to reduce the effect of this noise.

For incoherent processing, noise arises due to "self-clutter" introduced by the nonoverlapping portion of the sonic pulses (Pinkel and Smith 1992). The noise fractions of estimates from two adjacent "range bins" (3 m each) are partially correlated; however, bins separated by two or more intervals have uncorrelated Doppler noise (Pinkel and Smith 1992). This occurs regardless of system noise levels; for system noise, even adjacent estimates have uncorrelated noise. This suggests that the effects of noise can be offset by considering first cross-spectra formed between time series from two ranges along the same beam. The additional averaging employed in forming these cross-spectra works to reduce the effective noise level in the resulting coefficients, relative to the single-point values. This turns out to be a useful trick and is worth taking some time to explain.

a. Range-lagged cross-spectra

For purely progressive waves, the frequency cross-spectral coefficients from velocities measured at two distinct ranges would have magnitudes equal to those from the spectrum at either range alone. The phase of the range-lagged cross-spectrum would vary with frequency and would provide estimates of the projections of wavenumber along the beam, as a function of frequency. With varying depth, the speed and height of the waves varies; in this case the magnitude of the cross-spectrum would equal the geometric mean (square root of the product) of the two individual spectra. For waves that are not unidirectional, the cross-spectrum would decrease in magnitude with increasing separation of the two measurement locations relative to the geometric mean, as the directional components separate.

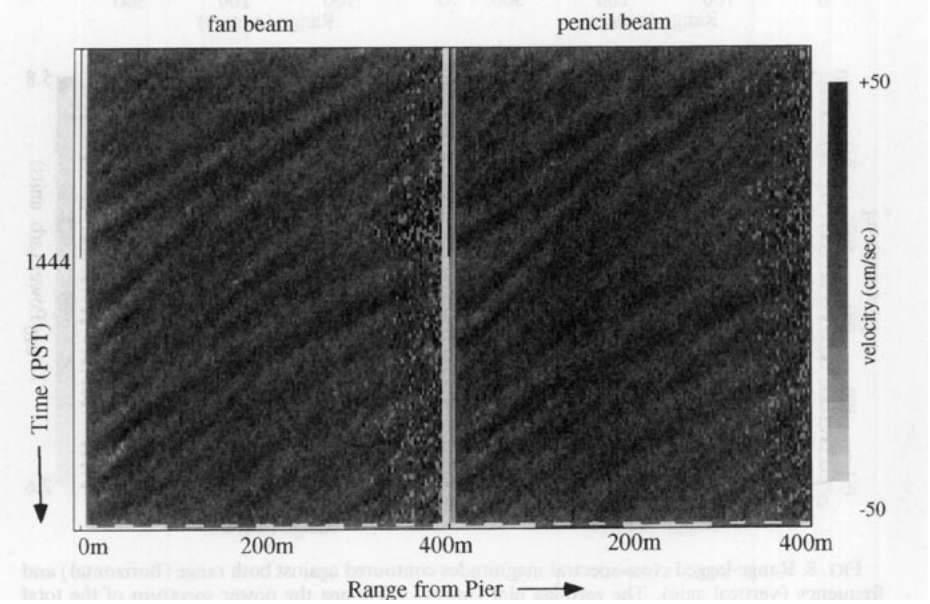

FIG. 7. An example of estimated velocities versus both time (vertical axis) and range (horizontal). The estimates from the two configurations are not noticeably different. Both appear fairly noisy. No signal coding was employed in this run. About 1 min of data is shown.

As noted above, estimates from adjacent range bins share some of the same noise contributions. The directional decorrelation effect argues for using minimum separation, while the Doppler noise correlation argues for using a separation of at least two range bins (6 m here). So two range bins appear optimal.

Figure 8 shows range-lagged cross-spectral magnitudes for several values of range separation (lags), using fan-beam data. These were formed from 36 min of data, sampled twice per second (4352 time samples) at each range. Time segments of 256 points were multiplied by a $\cos^2$ window and Fourier transformed, and then complex products were formed over the desired range pairs. The complex results were accumulated as the window was advanced 128 points at a time, yielding an average over 33 segments. As illustrated in Fig. 8, the apparent noise levels (e.g., for frequencies greater than 0.5 Hz) are greatly reduced at finite lag, relative to zero lag in range. To quantify this, the magnitudes were averaged over a representative "noisy" area for each range lag. Frequencies 35–128 (0.2734–1.0 Hz) and range bins 31–81 (93–243 m) were averaged together, giving a total of 4794 points per average. The results are most easily expressed in terms of $\log_{10}$ of the averaged magnitudes of the cross-spectra at the separations used (lags, or multiples of 3 m): lag 0: 2.1185; lag 1: 1.4490; lag 2: 1.3450; and lag 3: 1.3388 {in units of $\log_{10}$ $[(\text{cm s}^{-1})^2\ \text{Hz}^{-1}]$}. For reference, $10^{2.1185}$ times 1-Hz total bandwidth yields (11.46 cm $s^{-1})^2$ rms error, close to the above quoted estimate

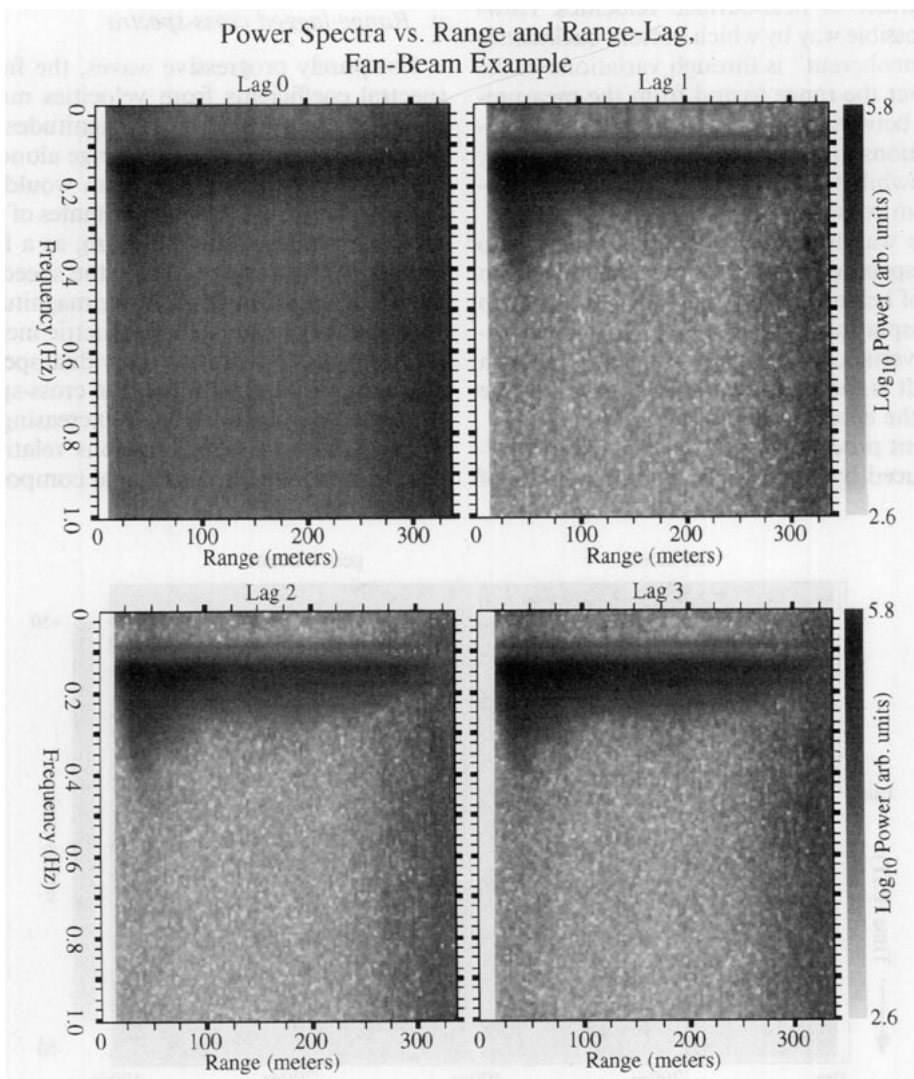

FIG. 8. Range-lagged cross-spectral magnitudes contoured against both range (horizontal) and frequency (vertical axis). The zero-lag plot [panel (a)] is just the power spectrum of the total received signal. At a range lag of one "bin" [3 m; panel (b)], some Doppler noise remains; however, it is greatly reduced relative to the zero-lag estimate. As the range lag is increased, some decorrelation is expected due to finite directional spread of the surface waves generating the signal, further decreasing the signal level [this is not apparent here; panels (c), (d)].

of $(12 \text{ cm s}^{-1})^2$. Again using 1-Hz total bandwidth, the other values yield equivalent rms velocity errors of lag 1: 5.30 cm s^{-1}; lag 2: 4.70 cm s^{-1}; and lag 3: 4.67 cm s^{-1}. The reduction in noise is greatest between lag 0 and lag 1, with some further improvement at lag 2 but little further reduction in variance at lag 3, consistent with the above discussion.

As further verification of the approach, the results from this range-lagged cross-spectral technique may be compared to the reduction in noise effected directly by use of repeat-sequence codes. To this end, spectra were formed and averaged in range for several different length repeat-sequence codes (Fig. 9). A range interval was selected over which the sonar performance appears reasonable (40–200 m). The magnitudes of the frequency cross-spectra formed at a range separation of 3 m (lag 1) were averaged together over this same range interval. The averaged magnitude of the frequency cross-spectrum is compared to the average of the geometric means of the frequency spectra at the corresponding pairs of ranges (Fig. 9). The difference between the cross-spectral magnitude and the geometric mean spectrum corresponds to the spectrum of the noise that is effectively removed in using the cross-spectra. These "residual spectra" are very nearly flat, as would be expected for Gaussian noise. Of interest here is the fact that the range-lagged cross spectra successfully reproduce the shapes of the true spectra over a substantial range of frequencies, even for the noisiest (uncoded) case (and as verified by the coded cases).

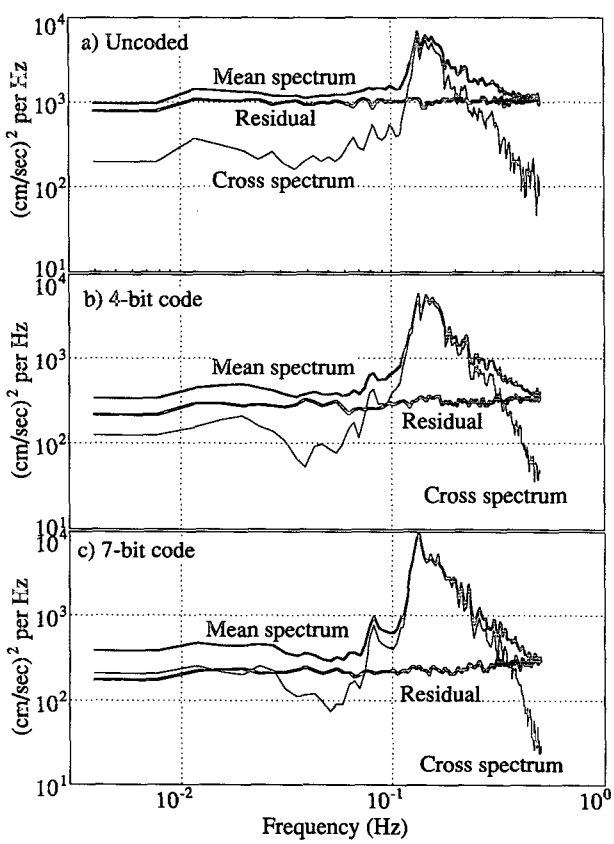

FIG. 9. Illustration of the cross-spectral method for reducing the Doppler noise in the spectral estimates (from averages over 40–200 m of the spectra shown in Fig. 8b). The magnitude of the averaged velocity cross-spectra at a fixed separation in range is compared to the mean spectrum. The difference between the cross-spectral magnitude and the mean spectrum is nearly flat in frequency, as is appropriate for a white-noise process. This greatly extends the band of usable frequencies for the analysis.

b. Cross-beam cross-spectra

With this background, we move to cross-spectra between the two kinds of beams. The "cross-beam cross-spectra" (as we shall call them) were formed with a range lag as well (of two range bins). These are compared with corresponding "lag 2" cross-spectra derived from each beam separately, as a function of both range and frequency (Fig. 10). The magnitudes of the range-lagged single-beam cross-spectra demonstrate the relative response of the two beams. At the nearest ranges, the pencil beam is well away from the surface, while the fan beam includes acoustic returns from the near-surface bright region. As seen in the illustration of the spectral magnitudes, it is only in this near-range region that the response differs; even here the difference is small. The near-range difference is consistent with the interpretation that the fan-beam signal comes from nearer to the surface than that of the pencil beam. The magnitudes of the cross-beam cross-spectra are not statistically different from the geometric means of the spectra from the individual beams; that is, the "signal part" of the coherence, as derived by use of range-lagged spectra, is very high. (In fact, cross-beam coherences fall almost exactly on the statistically expected levels for the given signal and noise levels.)

The phases of the cross-beam cross-spectral coefficients contain information about the position in range of an estimate from one beam relative to the position of the corresponding estimate from the other beam. In other words, each coefficient provides an estimate of the "apparent displacement" of one beam relative to the other. This provides another way to compare the two beams and thus to evaluate some additional possible effects of using a fan beam. In this nearshore scenario, the signal variance arises primarily from surface waves propagating shoreward, with a narrow angular spread. The change with range in the phase of a Fourier coefficient from a given beam is a direct measure of the wavenumber component along that beam, associated with the signal (due to surface waves) at that range and frequency. These "empirical wavenumbers" depend on the mean direction, directional spreading, and finite-depth effects on the waves, and each of these can vary with range. The changes with range and frequency can be determined empirically from either beam alone (and independently), using the range-

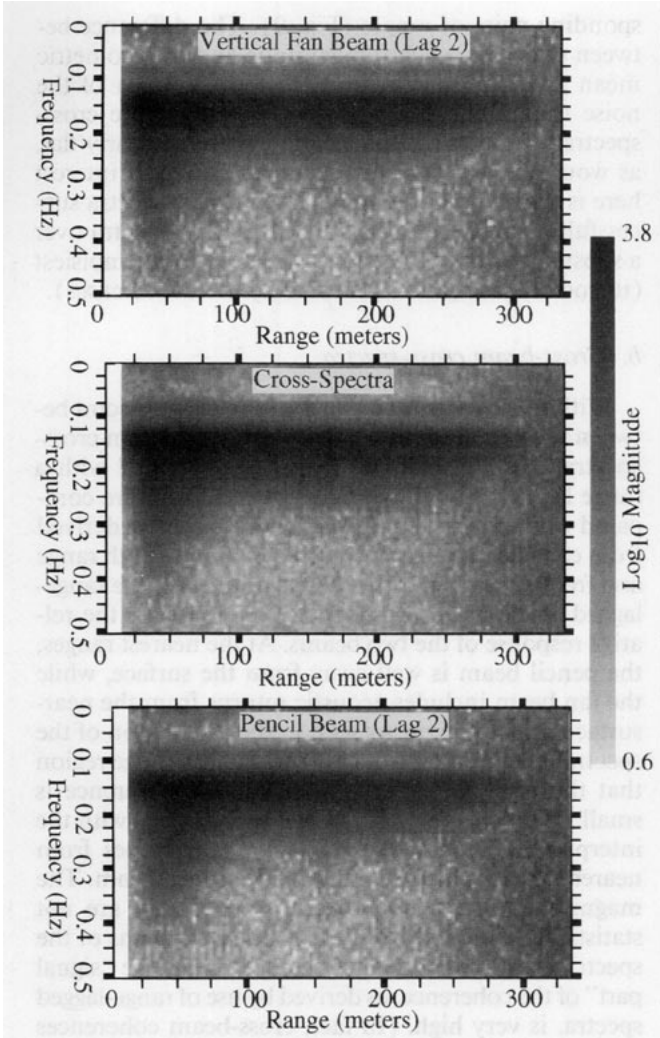

FIG. 10. Magnitudes of the cross-beam cross-spectra (center), compared to those of the range-lagged cross-spectra from each beam configuration (top and bottom). The cross-spectra are lagged in range by the same amount (2 bins or 6 m). The cross-beam magnitudes are almost identical to the geometric mean of the magnitudes from the two individual beams (differing only due to noise).

lagged single-beam cross-spectra discussed above. (The empirical wavenumbers derived from the two beams differ due to noise contributions but are quite similar wherever the wave signal is strong.) Next, the phase of the corresponding cross-beam cross-spectral coefficient may be taken to reflect the same empirical wavenumber. In this case, the phase of the cross-beam coefficient indicates an apparent range lag between the two measurements, which may (because of geometric effects) be different from the nominal separation. To deduce the apparent displacement between the measurements from the two beams, then, the phases of the cross-beam cross-spectral coefficients are compared to those for the same nominal separation along a single beam, for the corresponding frequency and range. A slight deficit or excess implies a displacement in the effective location of the measurement between the two beams. An average over a portion of the spectrum where the signal is strong yields a robust estimate of the effective displacement of one beam relative to the other.

The observed phases of the cross-beam correlations at nominally zero range displacements are shown in Fig. 11, contoured against both range and frequency. The derived range displacements are averaged over a selected frequency band, as suggested above, to estimate the interbeam displacement versus range. A frequency band is selected in which the surface wave signal dominates over noise, over as wide a range interval as practical. Figure 12 shows the displacement profiles resulting from an average over 0.14–0.22 Hz (frequency bins 18–28 out of 128, inclusive) and using the "empirical wavenumbers" derived from either the fan beam (thick lines) or the pencil beam (thin lines). Least-squares straight-line fits over ranges 60–180 m are also shown. This range interval was chosen by looking at Fig. 12 and selecting an interval over which the estimates appear least noisy. No particular trend with range is observed. The average displacement over 60–180 m in range is about -0.119 m $\pm$ 0.04 m using the fan-beam calibration, or -0.155 m $\pm$ 0.04 m using the pencil-beam calibration. The sense of this displacement is that the estimates from the fan beam appear to come from slightly closer ranges than those from the pencil beam but the displacement is just barely statistically significant.

To interpret the phase-derived range displacements, an estimate is needed of the difference in effective range, which should result in (for example) perfect reflections from both the surface and the bottom. A simple estimate is provided by averaging the horizontal component at each given radius ($r \cos\theta$, where θ is the elevation angle) over the estimated beam pattern (see Figs. 2 and 3). This corresponds roughly to the assumption that both the surface and bottom are perfect "mirrors." The beam patterns for the fan-beam and crossed-beam configurations were estimated using an idealized transducer bar, 1.47 cm $\times$ 50.1 cm, together with the acoustic center frequency of 195 kHz (Fig. 2). The inferred difference in the effective range of the measurements from the two beams would be about 0.87% of the nominal range, or 1–2 m at 100–200 m in range. From geometry, it is clear that this range discrepancy should increase directly in proportion to range. In contrast, the observed phases show no convincing trend with range (Fig. 12). The overall mean displacement over 60–180 m in range is -0.137 m $\pm$ 0.04 m. No rationalization for this constant displacement has been devised. In any case, it is negligible compared to both the nominal range resolution of 3 m and to the predicted difference in the presence of multiple reflections.

For the purpose of measuring surface waves, it appears that there is little advantage to using a pencil

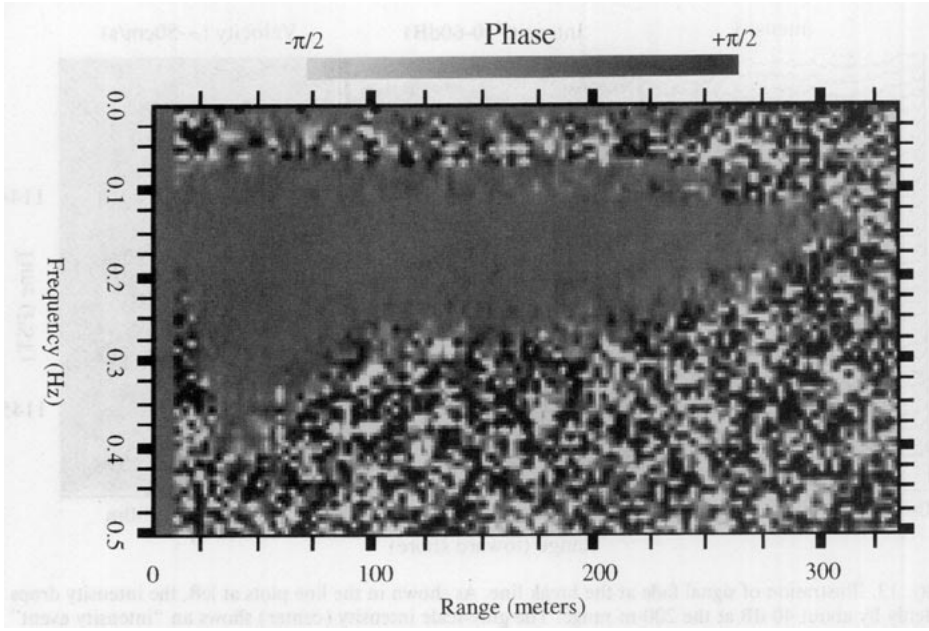

FIG. 11. Phase of the cross-beam cross-spectra, corrected to an equivalent nominal range displacement of zero between the two beams. Wherever the signal is strong (see Fig. 10), the phase is quite near zero (note magnified phase scale, ±90°).

beam. The fan beam is much more robust with respect to inexact placement of the instrument and small tilts introduced by shifting sediment. Also, the radial velocity estimates from the fan beam appear to be useful at a shorter range from the instrument package.

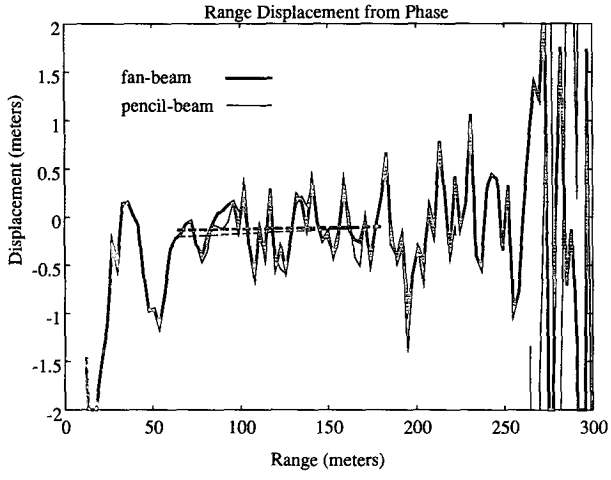

FIG. 12. Range displacement between the two beam configurations, calculated from the phase data of Fig. 11 and using reference phase versus displacement data from the fan beam (thick lines) or from the pencil beam (thin lines). For reference, least-squares straight-line fits are shown for the range interval 60–180 m. The trends do not indicate an increase in displacement with range. Negative values indicate that fan-beam data locations are displaced toward the instrument relative to the pencil beam.

5. Maximum range

The seaward-directed tests demonstrate a total range of about 400 m, with 5 m s^{-1} winds (e.g., Fig. 7). The range increases with transmitted power up to about 50 W (electrical) power output. As in the open sea, it is expected that the maximum range would decrease significantly in the absence of wind.

6. Minimum depth

The bottom at the test site is sandy and very flat between the sonar and the shore. The water depth decreases from 5 m at the sonar to about 1-m depth at the breakpoint of the waves. The shoreward-directed tests reveal some interesting features. The velocities appear to be useful up to the point where the incoming waves break; then there is about a 3-dB rise, followed by a tremendous drop in the returned intensity, and the velocity estimates "fade" (Fig. 13). This intensity cutoff at the breakpoint is observed also by Thorpe and Hall (1993), using 80-, 90-, and 250-kHz sound. At times, the wave orbital velocities appear to show a "phase jump." This can be close to 180° (Fig. 14) but not always. Apparently, the breaking waves have an enormous influence on the measurements. A plausible explanation for the observed features is that an extremely dense bubble cloud is produced by a plunging breaker. This first provides increased backscatter (by 3 dB or so), and also absorbs most of the sound (reducing the intensity by 30 dB or more thereafter). Another contender for the radical absorption of the sound

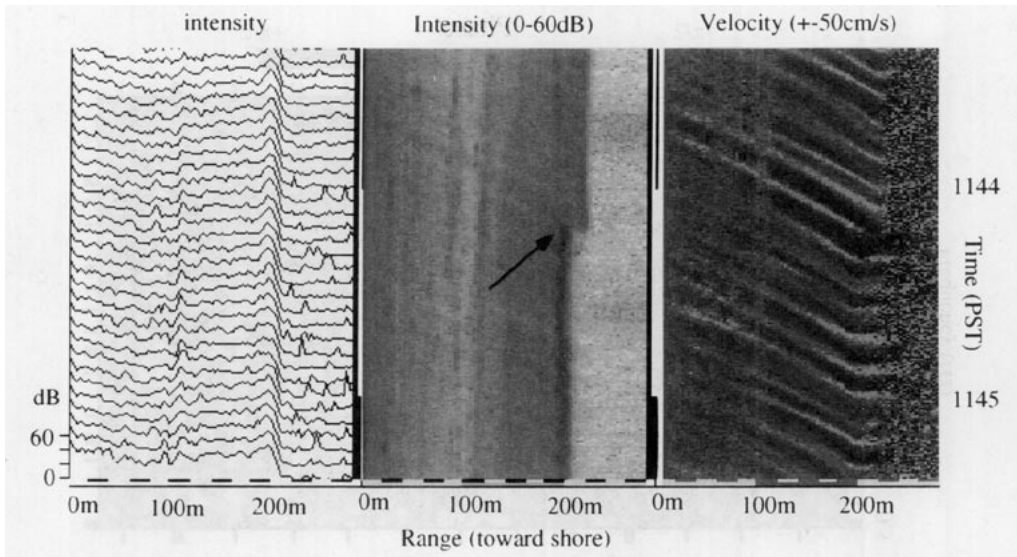

FIG. 13. Illustration of signal fade at the break line. As shown in the line plots at left, the intensity drops suddenly by about 40 dB at the 200-m range. The gray-scale intensity (center) shows an "intensity event" when an especially large wave breaks (arrow), with a subsequent shift seaward of the location of the intensity drop. Coincident with the intensity drop, the velocity "fades" as well (rightmost plot). Also, note the constant velocity versus range past the drop; this is due to the enormous reduction in sound speed in dense bubble clouds.

is sand, stirred up from the bottom by the plunging breakers (the waves were dependably of the plunging breaker form). The bubbles would also reduce the sound speed and could perhaps bring about reflection (due to the abrupt change in ρc) to account for the phase shifts sometimes observed. An alternative explanation for the apparent "phase jump" is that the radical absorption permits a reflection to be detected, which is normally hidden by the more slowly fading signal. For example, it is possible that one of the pier pilings was exactly behind the sonar, within the field of view of the less sensitive backward-directed beam pattern. This would produce a repetition of the final 20 m of data before the signal fade, at reduced intensity.

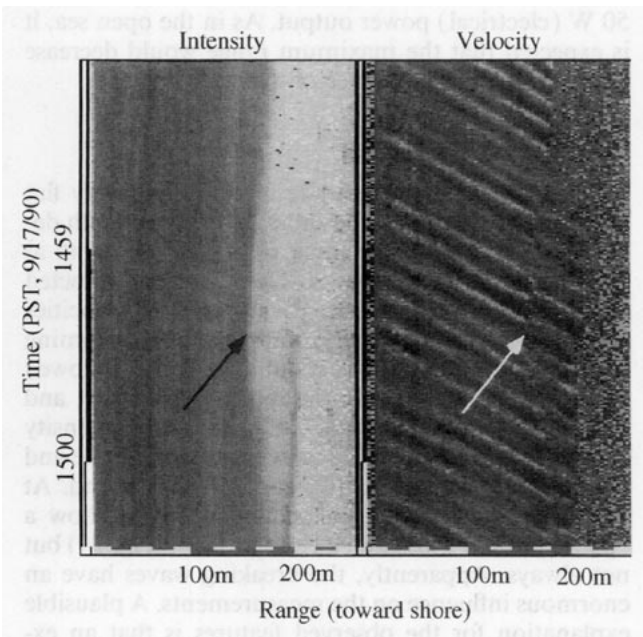

FIG. 14. An example of a velocity discontinuity at the breakpoint of the waves. Note that the velocity discontinuity is coincident with a significant drop in intensity (see arrows). Also, the boundary moves and evolves in time. Visually, this boundary appears to correspond to the division between white, foamy water shoreward of the breakpoint and the clear water outside.

7. Conclusions

The vertical fan beam performs well in the nearshore environment, from the breakpoint of the incoming waves seaward. Bottom reverberation and multiple-bounce effects appear to be negligible at 200 kHz and with at least 4 m s^{-1} wind. Caution should be exercised in extending these results to conditions other than those of the tests. In dead calm conditions, the bubbles may decrease to a level where the bottom reflections become detectable or even dominant. In any case, the accuracy of the velocity estimates determined here is in line with theoretical levels (Pinkel and Smith 1992), as well as with those observed with similar systems in the deep ocean.

Horizontally scanning Doppler sonar systems should prove useful in mapping a component of the horizontal velocity field over significant areas near shore. We look forward particularly to the application of the 45° "sector-scan" sonar to the near shore. The evolution in time of complex current patterns often found near

shore can now be studied in quantitative detail. New insights into the physics and dynamics of some of these processes should result.

Acknowledgments. This work was supported by the Physical Oceanography Division and by the Underwater Acoustics Division of the Office of Naval Research.

REFERENCES

Crawford, C. B., and D. M. Farmer, 1987: On the spatial distribution of ocean bubbles. *J. Geophys. Res.*, **92**, 8231–8243.

Herbers, T. H. C., and R. T. Guza, 1991: Wind-wave nonlinearity observed at the sea floor. Part I: Forced wave energy. *J. Phys. Oceanogr.*, **21**, 1740–1761.

——, and ——, 1992: Wind-wave nonlinearity observed at the sea floor. Part II: Wavenumbers and third-order statistics. *J. Phys. Oceanogr.*, **22**, 489–504.

——, R. L. Lowe, and R. T. Guza, 1991: Field verification of acoustic Doppler surface gravity wave measurements. *J. Geophys. Res.*, **96**, 17 023–17 036.

Inman, D. L., and B. M. Brush, 1973: The coastal challenge. *Science*, **181**, 20–32.

Lhermitte, R., and R. Serafin, 1984: Pulse-to-pulse coherent Doppler sonar signal processing techniques. *J. Atmos. Oceanic Technol.*, **1**, 293–308.

Pinkel, R., and J. Smith, 1992: Repeat sequence codes for improved performance of Doppler sounders. *J. Atmos. Oceanic Technol.*, **9**, 149–163.

Sherman, J. T., and R. Pinkel, 1991: Estimates of the vertical wavenumber–frequency spectra of vertical shear and strain. *J. Phys. Oceanogr.*, **21**, 292–303.

Smith, J. A., 1989: Doppler sonar and surface waves: Range and resolution. *J. Atmos. Oceanic Technol.*, **6**, 680–696.

——, 1992: Observed growth of Langmuir circulation. *J. Geophys. Res.*, **97**, 5651–5664.

Thorpe, S., 1986: Bubble clouds: A review of their detection by sonar, of related models, and of how K_v may be determined. *Oceanic Whitecaps*, D. Reidel, 57–68.

——, and A. J. Hall, 1983: The characteristics of breaking wave, bubble clouds, and near-surface currents observed using side-scan sonar. *Contin. Shelf Res.*, **1**, 353–384.

——, and ——, 1993: Nearshore side-scan sonar studies. *J. Atmos. Oceanic Technol.*, **10**, 778–783.

Weller, R. A., M. A. Donelan, M. G. Briscoe, and N. E. Huang, 1991: Riding the crest: A tale of two wave experiments. *Bull. Amer. Meteor. Soc.*, **72**, 163–183.